Atmos. Meas. Tech. Discuss., https://doi.org/10.5194/amt-2019-192
Manuscript under review for journal Atmos. Meas. Tech.
Discussion started: 17 May 2019

Atmospheric Measurement Techniques Discussions

The lightning flash rate per minute, calculated for big, medium, and small flashes together is displayed in the bottom graph of Fig. 12 in blue line. It remains rather weak with values lower than 10 m-1 until the end of the first main convective core at about 12:00 UT. Then, it exhibits several peaks between 12:00 UT and 13:00 UT with maxima of 48 min-1 at 12:20 UT, 33 min-1 at 12:28 UT, 47 min-1 at 12:34 UT, and 33 min-1 at 12:42 UT. Each of them corresponds to one of the convective surges reported in Table 2. The flash rate corresponding to small-isolated and short-isolated flashes is also displayed in the bottom graph of Fig. 12 in red line for comparison. Its maxima, greater than that of big, medium and small flashes considered together are also in phase with convective surges. The flash rate of small-isolated and short-isolated flashes is even the best proxy for the convective surges.

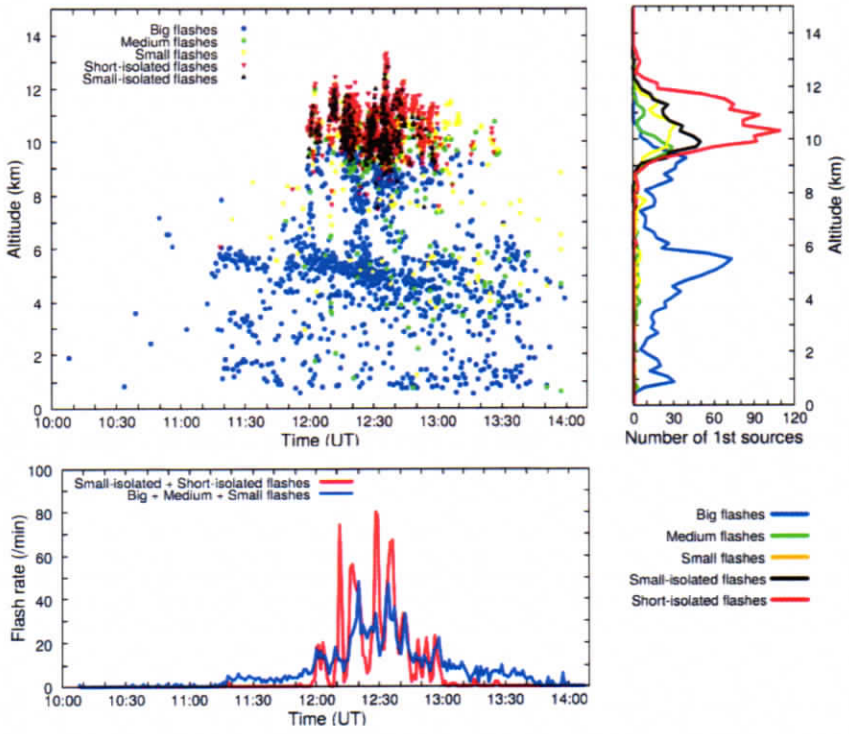

Figure 12: Altitude versus time of the first VHF sources of each flash during the whole 08/06/2015 MCS event (top left), altitude histogram of these first VHF sources with a vertical resolution of 200 m (top right), and 1-minute flash rate versus time (bottom) for Small-isolated and Short-isolated flashes (red) and for Big, Medium and Small flashes (blue).

The first sources of flashes have also been extracted via the XLMA flash algorithm in order to identify the preferential altitudes where lightning flashes were triggered. The altitude of those first sources are displayed versus time in the top left

Atmos. Meas. Tech. Discuss., https://doi.org/10.5194/amt-2019-192
Manuscript under review for journal Atmos. Meas. Tech.
Discussion started: 17 May 2019

Atmospheric Measurement Techniques Discussions

graph of Fig. 12 for each kind of lightning flash. Additional information about the number of first sources by flash type is given in the top right graph of Fig. 12 that provides their altitude histogram with a 200 m vertical resolution. The big flashes are triggered from the very beginning of the event until the end (blue dots in top left graph of Fig. 12). During the first convective core between about 11:10 UT and 12:00 UT the altitude of their first sources are distributed over 3 altitude levels (1.5 km, 3 km, and 5.5 km). The 2 lowest levels correspond mainly to Cloud-to-Ground flashes and the highest level to Intra-Cloud flashes. At 12:00 UT big flashes were suddenly triggered at a fourth altitude level laying between 8 km and 10 km high until the end of the more intense convective phase, i. e. 13:40 UT. Note that in the mean time from 12:00 UT to 12:40 UT the lowest first sources were much less numerous, this corresponds well to the intensification of convection and to a reduction in Cloud-to-Ground flash activity. After 13:40 UT big flashes were again only triggered at 3 altitude levels (1 km, 4 km, and 6 km). As far as medium and small flashes are considered, they were triggered at about all altitudes from 12:00 UT until the end of the event but much less numerous than big flashes, with however clear maxima at about 9.5 km and 10.7 km, respectively, during the phase of intense convection between 12:00 UT and 13:10 UT. During the same intensive period, numerous small-isolated and short-isolated flashes were triggered between 9 km and 13 km high. The altitude histograms in the top right graph of Fig. 12 show that big flashes triggering dominates at altitudes lower than 9 km (maximum of 73 first sources at 5500 m, i.e. between 5400 m and 5600 m). At higher levels corresponding to convective surges activity, big, medium, and small flashes exhibit maxima of 39 first sources at 9300 m, 29 first sources at 9700 m, 31 first sources at 10500 m, respectively (the smaller the flash the higher the altitude at which it is triggered), while small-isolated flashes and especially short-isolated flashes exhibit higher maxima of 50 first sources at 9900 m and 109 first sources at 10300 m, respectively. These results confirm the small scale electrical activity on top of convective core over small areas centered on convective surges positions indicated in Table 2. Furthermore, it seems that only small-isolated and short-isolated flashes are able to correctly account for this specific high level electrical activity associated with the uppermost part of convective surges.

4.2 Event of 8 June 2015: upper level discharges in the trailing stratiform region

During the same event of 8 June 2015, 6 uncommon flashes were detected by SAETTA in the trailing stratiform region of the mesoscale convective system (see Table 3 for detailed temporal and spatial characteristics); 4 of them were triggered during the second half of the phase of intense convection (between 12:00 UT and 13:10 UT, see Section 4.1); and the 2 others were triggered later during the decay phase. Those 6 flashes started like typical IC (or CG for one of them) via a bidirectional leader process (Kasemir, 1950; Israel, 1973; Mazur, 2002; Montanyà et al., 2015) the negative leader of which propagates upward until it reaches the upper positive charge of the regular dipole structure, then propagates away from the convective core into the stratiform region with a low descent associated with the sedimentation of the charged ice particles as described by Ely et al. (2008). However, during the propagation phase through the stratiform region, an upward positive leader - probably issued from a bileader triggered just above the positive charge layer of the stratiform region - suddenly

Atmos. Meas. Tech. Discuss., https://doi.org/10.5194/amt-2019-192
Manuscript under review for journal Atmos. Meas. Tech.
Discussion started: 17 May 2019

Atmospheric Measurement Techniques Discussions

appears at a distance varying from 14 km (flash #3) to 33 km (flash #2) from the convective core and propagates upward on a height varying from 3 km (flashes #2 and #3) up to 5 km (flash #5). Then the positive leader spreads in a negative charge layer almost horizontal but with a tilt parallel to that of the positive charge layer below, on altitudes ranging from a maximum of about 12 km to a minimum of about 8 km, and on horizontal distances varying from 10 km (flash #3) to 33 km (flash #5), in several directions even partly rearward (flash #5) but mainly downwind.

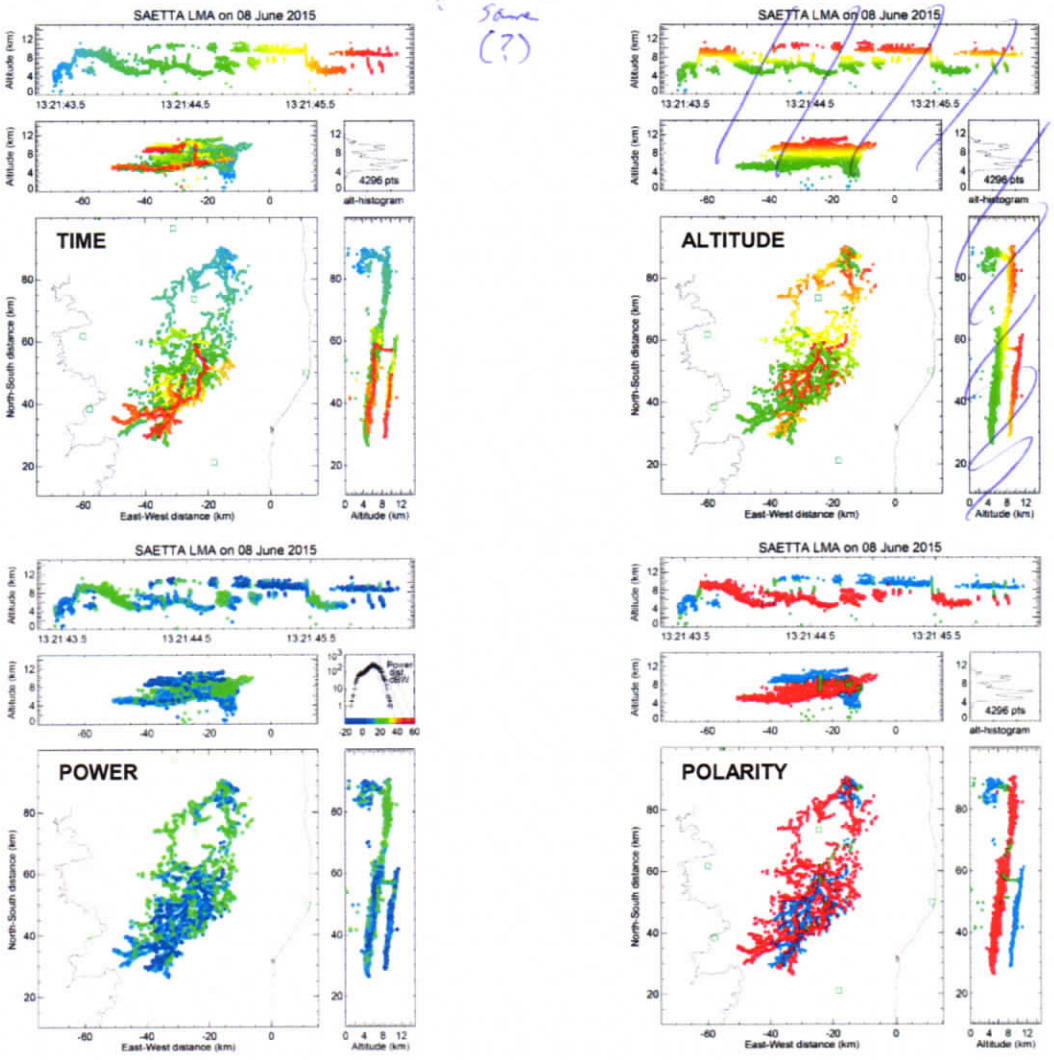

Figure 13: High altitude discharge in the stratiform region during the MCS event of 8 June 2015 at 13:21:43 UT. VHF sources displayed by dots with color scale corresponding to time (top left), altitude (top right), power (bottom left), and cloud charge polarity with positive in red, negative in blue (bottom right).

Atmos. Meas. Tech. Discuss., https://doi.org/10.5194/amt-2019-192
Manuscript under review for journal Atmos. Meas. Tech.
Discussion started: 17 May 2019

Atmospheric Measurement Techniques Discussions

Those uncommon flashes can be illustrated by flash #5 that appeared just before 13:21:43.5 UT. The corresponding VHF sources are displayed in Fig. 13 versus time (top left), altitude (top right), power (bottom left), and inferred cloud charge polarity (bottom right). The polarity of the VHF sources (selected by hand with the XLMA software) is deduced from the intensity of the power with which they are detected. Basically most powerful sources correspond to negative leaders that move through positively charged regions while less powerful sources correspond to positive leaders (actually negative recoil leaders) that move through negatively charged regions. This flash starts as a Cloud-to-Ground discharge that connects a negative charge layer located between about 4 km and 6 km altitude to the ground around the position defined by x = -14 km and y = 87 km, and shortly after develops as an intra-Cloud discharge with an upward negative leader that rises up to 9 km at 13:21:43.6 where it spreads in a positive charge layer. The propagation of the positive leader into the lower negative charge appears only until 13:21:43.8 while the negative leader travels through the whole stratiform region in a slowly tilted positive charge layer until 13:21:44.7. Before that, a first upward positive leader appears at 13:21:44.2 on top the positive charge layer at the position defined by x = -24 km and y = 57 km. This upward positive leader reaches the altitude of about 10 km and spreads horizontally. Probably 3 other upward leaders follow the same channel between 13:21:44.3 and 13:21:44.6. Later, 3 downward recoil discharges follow exactly the same path from the uppermost negative charge layer down to the positive charge layer of the stratiform region between about 13:21:45.5 and 13:21:46.1.

To further identify the discharges processes involved in that complex lightning flash, we performed the time-distance analysis proposed by van der Velde and Montanyà (2013). The calculated horizontal distance between the first source and each other source of the flash is displayed in Fig. 14 versus time in function of the altitude of the sources (top) and also in function of the cloud charge polarity in which the leaders propagate (bottom). In this way, one can easily refer to Fig. 13 (top right and bottom right) to identify the location of each discharge phase. The flash is constituted of 3 kinds of discharge processes according to the 3 kinds of slope that can be identified in Fig. 14. Note that positive slopes correspond to discharges propagating away from the first source meanwhile negative slopes correspond to discharge propagating toward the first source. On can first point out 4 main negative leaders (red lines in right graph) propagating away from the first sources in the stratiform region (increasing distance) and toward decreasing altitudes (color from orange to blue in left graph) with a rather fast radial speed of about 1.4×105 m s^{-1} (from 0.2 s to 0.75 s for the first one; from 1 s to 1.3 s for the second one; from 1.3 s to 1.45 s for the third one; and from 2 s to 2.3 s for the fourth one). Then, so-called positive leaders (negative recoil leaders) can be identified with a slower increasing distance with time mainly between 0.7 s and 2.7 s in blue color in right graph and in orange and red colors in left graph, i. E. they are localized at high altitude. The corresponding radial speed is about 1.7×10^4 m s^{-1}, which is one order of magnitude less than that of negative leaders. Those positive leaders correspond to the uncommon uppermost altitude discharges in the stratiform region. At last, one can identify very fast propagating discharges corresponding to the almost vertical lines in Fig. 14 at about 0.8 s; 1.5 s; 2.4 s; 2.5 s; 2.6 s; and between 1.5 s and 1.8 s, the radial speeds of which are about 106 m s-1 (between 8×10^5 m s^{-1} and 1.4×10^6 m s^{-1}). Those fast

Atmos. Meas. Tech. Discuss., https://doi.org/10.5194/amt-2019-192
Manuscript under review for journal Atmos. Meas. Tech.
Discussion started: 17 May 2019

Atmospheric Measurement Techniques Discussions

propagating discharges may be dart leaders or long recoil events according to van der Velde and Montanyà (2013). The latter can be distinguished at the end of the flash sequence in the top left graph of Fig. 13: The discharge propagates 3 times consecutively from the south tip of the upper most layer of VHF sources, returns northward to the vertical channel of the initial ascending leader, descend this channel and propagate southward in the positive charge of the stratiform region (in orange and red). As a matter of fact, the successive passages of these events through the vertical channel can be illustrated by the green dots present in each of the almost vertical lines in the bottom graph of Fig. 13. All the radial speeds here evaluated are in good agreement with previous observational studies; see van der Velde and Montanyà (2013) for a review.

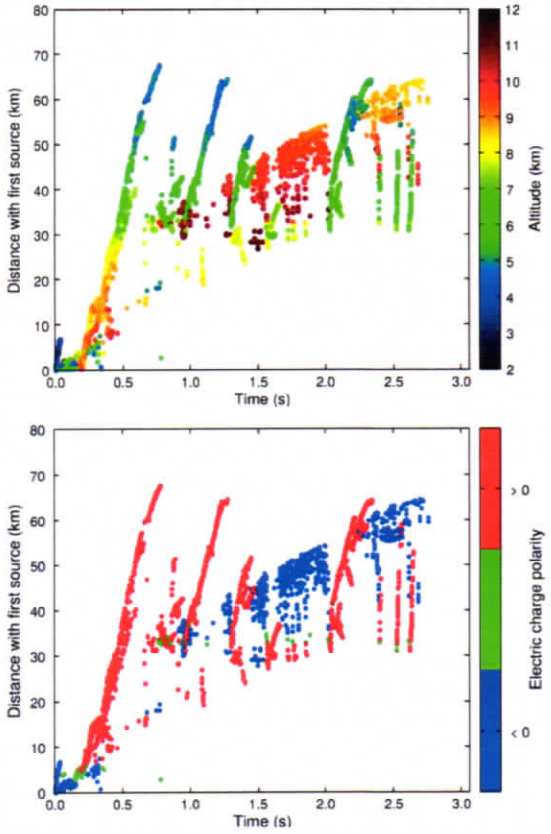

Figure 14: High altitude discharge in the stratiform region during the MCS event of 8 June 2015 at 13:21:43 UT. Horizontal distance between each VHF source and the first source versus time in function of altitude (top) and cloud charge polarity in which the leaders propagate (bottom). The time is indicated in seconds from the beginning of the flash.

Several questions arise from the observation of such a complex lightning flash involving 2 layers of charge in the trailing stratiform region. How a positive leader can propagate upward from the top of the main positive charge layer in that region?

Atmos. Meas. Tech. Discuss., https://doi.org/10.5194/amt-2019-192
Manuscript under review for journal Atmos. Meas. Tech.
Discussion started: 17 May 2019

What are the mechanisms involved in the formation of the uppermost negative charge layer in that region? Why all MCS do not exhibit such complex lightning flashes? The most important process than can bring pertinent answers to these questions is probably the establishment of the uppermost layer of negative charge. One can refer to the review by Stolzenburg and Marshal (2008) on the charge layers structure in such convective systems, based from in situ balloon-borne measurements. As observed in present study, lightning in convective systems are most often triggered in or near the convective cores (Ribaud et al., 2016) and can subsequently propagate horizontally into the anvil or into the trailing stratiform region (Carey et al., 2005; Dotzek et al., 2005; Tessendorf et al., 2007; MacGorman et al., 2008), following the path of charged ice particles that sediment (Carey et al., 2005; Ely et al., 2008). Kuhlman et al. (2009) reported observations of in-cloud development of lightning flashes in the anvils of 2 supercell storms. They showed that the convergence of the anvils with opposite polarities of charge at the same altitude could increase electric field magnitude and favor the initiation of distant anvil lightning. But lightning activity in anvils at earlier and latter times was rather supposed to result from some charging mechanism that would be active in anvil as suggested by Dye and Willett (2007), i.e. that anvil charge would not necessarily originate from transport from the convective core. They also made a comparison with the high electrification of stratiform precipitation regions of mesoscale convective systems where extensive lightning activity develops horizontally (Dotzek et al., 2005, MacGorman et al. 2008) as in the anvils they observed. Recently, Dye and Bansemer (2018, 2019) proposed a conceptual model of mesoscale updraft covering extensive and deep areas during long periods, with non-riming ice collisional charging at mid to upper levels in absence of supercooled liquid water (Luque et al., 2016), in which larger particles carrying one charge (here positive) fall relative to the smaller particles particle carrying the opposite charge (here negative). Reaching a balance level near the top of the cloud where the updraft has became weak, the small particles with low terminal velocities would accumulate at that level while larger particles with terminal velocities greater than the updraft would sediment downward in the cloud. This scenario would result in the presence of a narrow layer of charge (here negative) near the top of the cloud and a thicker layer of charge (here positive) 2 to 3 km below, in a 30 min time period.

Present observation of the 8 June 2015 mesoscale convective system supports very well the conceptual model of Dye and Bansemer (2018, 2019), i.e. presence of a thin upper layer of negative charge above a thick mid-level layer of positive charge in the trailing stratiform region. The geometrical characteristics of the thin upper layer of negative charge must though be confronted to further analysis. For example, are (i) the horizontal extension (33 km) of this upper layer, (ii) the height (5 km) of the vertical channel through which the discharge connects the two layers, and (iii) the slope of the upper thin layer, consistent with this model of mesoscale updraft? Couldn't the thin upper layer of negative charge originate from a screening effect by electrostatic influence from above the cloud (Marshall et al., 1989; Wiens et al., 2005)? All these questions remain open and could benefit from a modeling study with a mesoscale cloud resolving model.

Besides, one can wonder if the first convective core that appeared between 11:12 UT and 12:03 UT about 20 km to the South of the 2 other main convective cores could have played a part in the subsequent charge structure of the trailing stratiform

Atmos. Meas. Tech. Discuss., https://doi.org/10.5194/amt-2019-192
Manuscript under review for journal Atmos. Meas. Tech.
Discussion started: 17 May 2019

Atmospheric Measurement Techniques Discussions

region in which it was embedded. Actually it was still active when those other cores developed (11:44 UT and 11:52 UT). They produced their first long range lightning that propagated in their common stratiform region at 12:09:56 UT, i.e. only 7 min after the end of the electrical activity of the first convective core, and produced their first uncommon high altitude discharge (flash #1 in Table 3) at 12:38:39, i.e. about 30 min later. Therefore, the interaction of this first convective core with the subsequent common trailing stratiform region of the two other cores should be further explored. On the same way, one could also consider the interaction between both trailing stratiform regions associated with each of the two main convective cores.

Flash	Flash type	Time (UT)	Duration (s)	First source altitude (km)	Convective core position		Upper level vertical branch heigh (km)	Vertical branch position		Distance from vertical branch to convective core (km)	Upper level discharge horizontal extension (km)
					x (km)	*y* (km)		*x* (km)	*y* (km)		
# 1	IC	12:38:39	1.8	8	-16	74	3.5	-17	56	18	16
# 2	IC	12:43:02	2.0	8	-41	77	3	-28	47	33	18
# 3	IC	12:54:05	1.7	7.5	-14	77	4	-23	66	14	10
# 4	IC	12:59:20	2.5	7	-43	72	3	-43	46	26	22
# 5	CG/IC	13:21:43	2.8	4	-14	87	5	-24	57	31	33
# 6	IC	13:57:18	1.7	5	-39	84	3	-24	59	29	21

Table 3. Time and spatial characteristics of the 6 upper level discharge observed by SAETTA in the stratiform region of the 8 June 2015 mesoscale convective system.

5 Conclusion and perspectives

Corsica is a very suitable place to study convection in maritime and mountainous environment but also to observe the climate trend of convection in Mediterranean region supposed to be a climatic hot spot (Giorgi, 2006). In 2014, 12 LMA stations constituting the SAETTA network were deployed there to carry out the monitoring of the total lightning activity at high spatial and temporal resolutions. The network has been operational since the summer of 2014, with winter interruptions in the first two years and then permanent operation since April 2016, with the project of operating on long term to try to observe climatic trends. As far as we know, SAETTA is the first LMA network deployed on such a rough terrain with a range of altitude on about 2000 m.

Atmos. Meas. Tech. Discuss., https://doi.org/10.5194/amt-2019-192
Manuscript under review for journal Atmos. Meas. Tech.
Discussion started: 17 May 2019

In order to explore the performances of SAETTA we evaluated its geometric potential of VHF sources detection by at least 6 stations considering the mask effect of the relief. This is the first time such an exercise has been done for a network of LMA stations. We found that in the range of about 120 km from the center of Corsica, the minimum altitude above which a VHF source can be detected is almost everywhere less than 2 km on average except in some sectors in the south and south-east of Corsica where this altitude can rise 4 to 5 km beyond about 100 km from the center of the island. This potential logically deteriorates when the 3 highest stations are off for wintering from December to March, with a south-west region very poorly documented beyond 100 km from the center of the island (minimum altitude greater than 6-9 km). We also evaluated its detection accuracy by means of the geometric model of Thomas et al. (2004) and we compared the results with those concerning the STEPS network (Lang et al., 2004; Thomas et al., 2004). The performances seem very similar (and even better for the slant range) albeit the SAETTA network is much more geographically extended for the same number of stations. The contribution of the vertical base of this mountainous network compared to a totally flat network shows also that the accuracy is significantly improved ~~on the altitude of the~~ sources beyond 150 km. A more comprehensive assessment of SAETTA's performance could undoubtedly benefit from comparisons with the trajectories of airliners that are detected by the network. We plan to perform this kind of comparison with GPS data of commercial flights.

Combining observations from the years 2004 to 2006, we have elaborated a short of climatology of total lightning activity on Corsica, which has never been done so far, in a 240 km × 240 km domain. The number of lightning days per square kilometer is dominated by daytime convection over the relief from June to July, with a local maximum at the north center of the island produced in July between 11:00 UT and 14:00 UT. Tidiga et al. (2018) showed - via a numerical study using the cloud resolving model Meso-NH at high resolution - that in absence of synoptic forcing this local maximum is likely due to the low-level convergence of moist air fluxes originated from sea breezes channeled through three main valleys that converge towards each other at this place. Subsequent studies envisaged should analyze the fine-scale impact of synoptic forcing on this scenario. Besides, the monthly number of lightning days undergoes two maxima: (i) one in June due to daytime convection in phase with the maximum of solar flux at the summer solstice; (ii), and one in September associated with numerous small storms over the sea or with some high precipitation events. Those last events may be associated with high precipitation and flash floods (Scheffknecht et al, 2016) and are the focus of the HyMeX program (Ducrocq et al., 2014).

The present paper also reports unusual lightning events that occurred in a mesoscale convective system on June 8, 2015. Produced during convective surges, the first type of lightning events was constituted of numerous VHF sources concentrated on a small perimeter (5 km by 5 km) and protruding from the top of the cloud located at about 11.5 km, up to 14 km from altitude. They correspond to a quasi continuous activity of positive leaders of very limited vertical and horizontal extension reaching an upper layer of negative charge, i. e. probably the typical uppermost charge region in MCS structure (Stolzenburg et al., 1998). The implementation of the XLMA flash algorithm of Thomas et al. (2003) shows that most of these lightning

Atmos. Meas. Tech. Discuss., https://doi.org/10.5194/amt-2019-192
Manuscript under review for journal Atmos. Meas. Tech.
Discussion started: 17 May 2019

Atmospheric Measurement Techniques Discussions

activity is constituted of small-isolated and especially short-isolates flashes, which are most commonly disregarded in flashes classification. The second type of lightning events concerns uncommon high altitude discharges in the trailing stratiform region of the mesoscale convective system. A focus is made on one of them that started as a cloud-to-ground flash, propagates upward with a negative leader reaching the upper positive charge of the cloud, then propagates away from the convective core into the stratiform region with a low descent. But suddenly a positive leader rises vertically 31 km away of the convective core and over 5 km to reach an uppermost thin layer of negative charge, with multiple subsequent recoil phases between this uppermost negative charge layer and the underneath main positive charge layer. Such a complex flash has never been published to our knowledge. Interestingly, this type of flash seems to confirm the recent conceptual model of Dye and Bansemer (2018, 2019) that explain such upper level layer of charge in the stratiform region by the action of a non-riming ice collisional charging in a mesoscale updraft.

SAETTA is now a high performance lightning 3D imager that can serve as a reference for electrical schemes of Meso-NH cloud resolving model (Barthe et al., 2012; Pinty et al., 2013), for operational LF/VLF lightning location systems in this region, for measurement campaigns such as EXAEDRE (https://www.hymex.org/exaedre/) that took place in Corsica in September and October 2018, but also for the calibration/validation phases of the future observations performed by the optical lightning imager LI on the Meteosat Third Generation geostationary platform (Eumetsat) that will be launched in the forthcoming years.

Appendix A : geometrical potential of VHF source detection by SAETTA

In this appendix we describe the geometric method used to estimate the minimum altitude at which a VHF source can be detected by the SAETTA network in a 240 km × 240 km square area centered on Corsica, with a 5 km horizontal resolution (48 × 48 pixels). All altitudes are here considered above mean sea level (AMSL) and the Earth radius RE is assumed uniform on the domain. The location of SAETTA stations is provided by their GPS positioning system; their altitude is derived from the data set of the National Institute of Geographical and Forest Information (IGN) via the Geoportail website (https://www.geoportail.gouv.fr/). All geographic positions are converted to Cartesian coordinates using Lambert's conformal conic projection for France (Duquenne et al., 2005). The relief of Corsica is obtained by interpolation – by the Cressmann method with a horizontal resolution of 100 m – of the SRTM digital elevation data (SRTM 90m Digital Elevation Database v4.1) of the Consortium for Spatial Information CGIAR-CSI (http://www.cgiar-csi.org/data).

The algorithm implemented for this calculation is as follows (see Fig. A1 to identify the different variables named hereafter): (i) a point Px at an altitude z_{Px} above a given pixel is considered; (ii) one looks at whether the direct line of sight between this point Px and each of the SAETTA stations (point St of altitude z_{St}) intersects the terrain of altitude z_r or not (for that the altitude z_P of each point P distributed every 1 km along each line of sight is compared to z_r); (iii) if the considered point is

Atmos. Meas. Tech. Discuss., https://doi.org/10.5194/amt-2019-192
Manuscript under review for journal Atmos. Meas. Tech.
Discussion started: 17 May 2019

Atmospheric Measurement Techniques Discussions

visible by less than 6 SAETTA stations, its altitude is increased (increment of 500 m); (iv) the sequence (iii) is repeated as long as the considered point is visible by less than 6 stations; (v) when the considered point is visible by at least 6 stations, its altitude z_{Px} is the solution for the given pixel and one moves to another pixel.

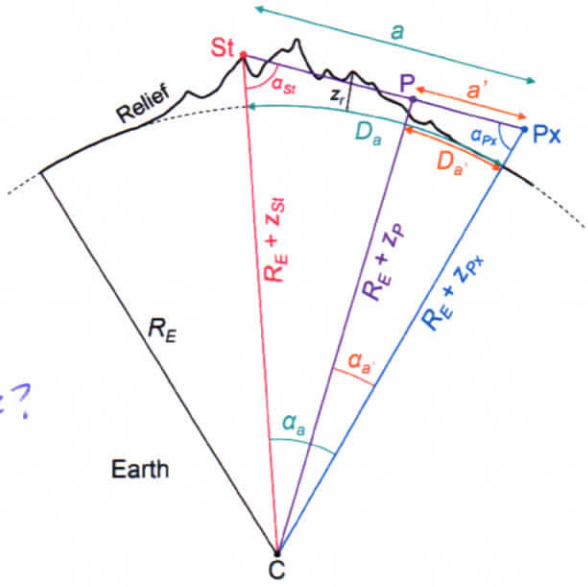

5

Figure A1: Geometry used in the calculations carried out to evaluate the geometric potential of VHF sources detection by the SAETTA network

The main difficulty that arises in this calculation is to determine the altitude z_P of each point P along the direct line of sight
10 (Px, St) by taking account the roundness of the Earth, the center of which is the point C. Here is how the calculation was conducted. According to Fig. A1, D_a stands for the known geographic distance between the pixel and the station, and $D_{a'}$ stands for the known geographic distance between the pixel and the point P along the line of sight. Assuming the Earth curvature is uniform on the domain, one can deduce the corresponding angles α_a and $\alpha_{a'}$:

$$\alpha_a = \frac{D_a}{R_E} \quad \text{and} \quad \alpha'_a = \frac{D'_a}{R_E} \qquad \text{(A1)}$$
15

Then, the distance a between the points St and Px is deduced from the generalized Pythagorean theorem applied to the triangle (C, St, Px) according to the following expression.

Atmos. Meas. Tech. Discuss., https://doi.org/10.5194/amt-2019-192
Manuscript under review for journal Atmos. Meas. Tech.
Discussion started: 17 May 2019

Atmospheric Measurement Techniques Discussions

$$a^2 = (R_E + z_{St})^2 + (R_E + z_{Px})^2 - 2(R_E + z_{St})(R_E + z_{Px})\cos\ \alpha_a \quad \text{(A2)}$$

Using the law of sines in that triangle (C, St, Px):

$$\frac{R_E + z_{St}}{\sin\ \alpha_{Px}} = \frac{R_E + z_{Px}}{\sin\ \alpha_{St}} = \frac{a}{\sin\ \alpha_a} \quad \text{(A3)}$$

we can deduce the angles α_{St} and α_{Px}:

$$\sin\ \alpha_{St} = \sin\ \alpha_a \times \frac{R_E + z_{Px}}{a} \quad \text{and} \quad \sin\ \alpha_{Px} = \sin\ \alpha_a \times \frac{R_E + z_{St}}{a} \quad \text{(A4)}$$

Using the law of sines in the triangle (C, St, P) gives:

$$\frac{R_E + z_P}{\sin\ \alpha_{St}} = \frac{a - a'}{\sin\ (\alpha_a - \alpha'_a)} \quad \text{(A5)}$$

did not confirm your math as (A2) ⇒ (A7)

Using the law of sines in the triangle (C, P, Px) gives:

$$\frac{R_E + z_P}{\sin\ \alpha_{Px}} = \frac{a'}{\sin\ \alpha'_a} \quad \text{(A6)}$$

By isolating a' in equation A6 and returning its expression in equation A5, we obtain the unknown z_P that we are looking for:

$$z_P = \frac{a}{\frac{\sin\ (\alpha_a - \alpha'_a)}{\sin\ \alpha_{St}} + \frac{\sin\ \alpha'_a}{\sin\ \alpha_{Px}}} - R_E \quad \text{(A7)}$$

Fig. A2 illustrates the determination of the minimum altitude at which a considered point (here the southwest corner of the domain corresponding to the zero abscissa) can be seen from one SAETTA station (here the Aleria station located on the East coast). The red lines correspond to lines of sight that intersect the relief meanwhile the blue line corresponds to the first

Atmos. Meas. Tech. Discuss., https://doi.org/10.5194/amt-2019-192
Manuscript under review for journal Atmos. Meas. Tech.
Discussion started: 17 May 2019

Atmospheric Measurement Techniques Discussions

altitude (here 12500 m) at which the considered point can be seen by the SAETTA station. The curvature of the lines illustrates the influence of the roundness of the Earth. → This approach was used to produce the results shown in Fig 2.

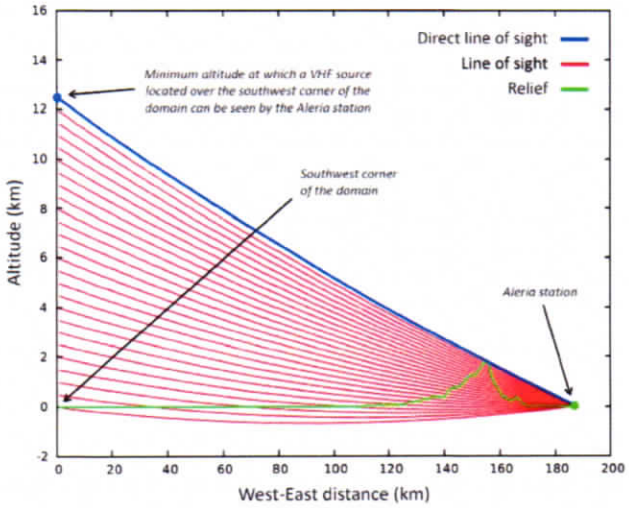

Figure A2: Illustration of the search algorithm for the minimum altitude of direct vision between a pixel and a station (e.g. here between the southwest corner of the domain and the Aleria station on the East coast) taking into account the earth's roundness.

Appendix B : XLMA Flash Algorithm Options

Max spatial separation for points in a flash (m)	3000.0
Max altitude separation for points in a flash (m)	5000.0
Max time separation for points in a flash (s)	0.15
Max allowable flash length (s)	3.0
Min acceptable vertical velocity (m/s)	20000.0
Max number of points in a flash group	50000.0
Lat Lon pixel size for density ratios and size	0.01
Max number of points to be a small flash	10
Point division between medium and big flashes	75
Max number of points in a flash fragment or noise	3
Ratio of number of points between parent and fragment	15
Max difference in azimuth between parent and fragment (rad)	0.05

Fraction of spatial separation for sparce connection	0.50
Min number of points in a sparce connection	3
Max score for noise	2
Normal IC altitude (m) divider (75% must be greater than)	5500.0
Low flash altitude (m) divider (75% must be less than)	7000.0
Rejoin flashes?	yes

Acknowledgments

Acknowledgements are addressed to SAETTA main sponsors: Collectivité Territoriale de Corse through the Fonds Européen de Développement Régional of the European Operational Program 2007-2013 and the Contrat de Plan Etat Région that funded the CORSiCA project; Collectivité de Corse through the CORSiCA 2017-2019 project; CNRS-INSU through the HyMeX/MISTRALS program; ANR IODA-MED; CNES through the SOLID project; UPS/Observatoire Midi-Pyrénées; and Laboratoire d'Aérologie. We also strongly thank the many individuals and regional institutions in Corsica (including the Conservatoire du Littoral, Qualitair Corse, and INRA San Giuliano) who host the 12 stations of the network, who helped us to find sites, or who bring us assistance for the logistics during missions in the field.

References

Adler, B., Kalthoff, N., Kohler, M., Handwerker, J., Wieser, A., Corsmeier, U., Kottmeier, C., Lambert, D., and Bock, O.: The variability of water vapour and pre-convective conditions over the mountainous island of Corsica: Q. J. R. Meteorol. Soc., DOI:10.1002/qj.2545, 2015.

Barthe, C., Chong, M., Pinty, J.-P., Bovalo, C., and Escobar, J.: CELLS v1.0: updated and parallelized version of an electrical scheme to simulate multiple electrified clouds and flashes over large domains, Geosci. Model Dev., 5, 167-184, doi.org/10.5194/gmd-5-167-2012, 2012.

Barthlott, C., Adler, B., Kalthoff, N., Handwerker, J., Kohler, M., and Wieser, A.: The role of Corsica in initiating nocturnal offshore convection, Q. J. R. Meteorol. Soc., DOI:10.1002/qj.2415, 2014.

Carey, L. D., Murphy, M. J., McCormick, T. L., and Demetriades, N. W. S.: Lightning location relative to storm structure in a leading-line, trailing-stratiform mesoscale convective system, J. Geophys. Res., 110, D03105, doi:10.1029/2003JD004371, 2005.

Chmielewski, V. C., and Bruning, E. C.: Lightning Mapping Array flash detection performance with variable receiver thresholds, J. Geophys. Res. Atmos., 121, 8600–8614, doi:10.1002/2016JD025159, 2016.

Cummins, K.L., Murphy, M. J., Bardo, E. A., Hiscox, W. L., Pyle, R. B. E., and Pifer, A. E.: A combine TOA/MDF technology upgrade of the U.S. National Lightning Detection Network, J. Geophys. Res. 103, 9035–9044, 1998.

Dotzek, N., Rabin, R. M., Carey, L. D., MacGorman, D. R., McCormick, T. L., Demetriades, N. W., Murphy, M. J., and Holle, R. L.: Lightning activity related to satellite and radar observations of a mesoscale convective system over Texas on 7 – 8 April 2002, Atmos. Res., 76, 127 – 166, doi:10.1016/j.atmosres.2004.11.020, 2005.

Ducrocq, V., Nuissier, O., Ricard, D., Lebeaupin, C., and Thouvenin, T.: A numerical study of three catastrophic precipitating events over southern France. II: Mesoscale triggering and stationarity factors, Q. J. R. Meteorol. Soc. 134: 131–145, 2008.

Ducrocq, V., et al.: HyMeX, les campagnes de mesures : focus sur les événements extrêmes en Méditerranée (in French), La Météorologie, 37-47, n° 80, février, 2013.

Ducrocq, V., et al.: HYMEX-SOP1 The Field Campaign Dedicated to Heavy Precipitation and Flash Flooding in the Northwestern Mediterranean, Bull. Am. Meteorol. Soc., 1083-1100, July, DOI:10.1175/BAMS-D-12-00244.1, 2014.

Duquenne, F., Botton, S., Peyret, F., Betaille, D., and Willis, P.: GPS, Localisation et Navigation par Satellite, 2nd edition, Hermes Sciences, Lavoisier, 2005.

Dye, J. E., and Willett, J. C.: Observed enhancement of reflectivity and electric field in long-lived Florida anvils, Mon. Weather Rev., 135, 3362-3380, doi:10.1175/MWR3484.1, 2007.

Dye, J. E., and Bansemer, A.: Observations of electrification in deep, precipitating stratiform clouds, proc. of the 16th Int. Conf. on Atmospheric Electricity, June 17-22, Nara, Japan, 1-10, 2018.

Dye, J. E., and Bansemer, A.: Electrification in mesoscale updrafts of deep stratiform and anvil clouds in Florida. J. of Geophys. Res. Atmos., 124, 1021–1049, doi.org/10.1029/2018JD029130, 2019.

Ely, B. L., Orville, R. E., Carey, L. D., and Hodapp, C. L.: Evolution of the total lightning structure in a leading-line, trailing-stratiform mesoscale convective system over Houston, Texas, J. Geophys. Res., 113, D08114, doi:10.1029/2007JD008445.

Fuchs, B. R., Rutledge, S. A., Bruning, E. C., Pierce, J. R., Kodros, J. K., Lang, T. J., MacGorman, D. R., Krehbiel, P. R., and Rison, W.: Environmental controls on storm intensity and charge structure in multiple regions of the continental United States, J. Geophys. Res. Atmos., 120, 6575-6596, doi:10.1002/2015JD023271, 2015.

Giorgi, F.: Climate change hot-spots, Geophys. Res. Let., Vol. 33, L08707, doi:10.1029/2006GL025734, 2008.

Israel, H.: Atmospheric Electricity, Vol. II (translated from German), published by the National Science Foundation, Washington, DC by the Israel Program for Scientific Translations, 1973.

Kasemir, H. W.: Qualitative Ubersicht uber Potential-, Feld- und Ladungsverhaltnisse bei einer Blitzentladung in der Gewitterwolke (Qualitative Survey of the Potential, Field and Charge Conditions during a Lightning discharge in the Thunderstorm Cloud), in: H. Israel (Ed.), Das Gewitter, Leipzig, Akadem. Verlagsgesellschaft, 1950.

Koshak, W. J., et al.: North Alabama Lightning Mapping Array (LMA): VHF source retrieval algorithm and error analyses, J. Atmos. Oceanic Technol., 21, 543– 558, 2004.

Kuhlman, K. M., MacGorman, D. R., Biggerstaff, M. I., and Krehbiel, P. R.: Lightning initiation in the anvils of two supercell storms, Geophys. Res. Lett., 36, L07802, doi:10.1029/2008GL036650, 2009.

Lambert, D., and Argence, S.: Preliminary study of an intense rainfall episode in Corsica, 14 September 2006. Adv. Geosci., 16, 125–129, 2008.

Lambert, D., Mallet, M., Ducrocq, V., Dulac, F., Gheusi, F., and Kalthoff, N.: CORSiCA: a Mediterranean atmospheric and oceanographic observatory in Corsica within the framework of HyMeX and ChArMEx. Adv. Geosci., 26, 125–131, 2011.

Lang, T., Miller, L. J., Weisman, M., Rutledge, S. A., Barker III, L. J., Bringi, V. N., Chandrasekar, V., Detwiler, A., Doesken, N., Helsdon, J., Knight, C., Krehbiel, P., Lyons, W., MacGorman, D., Rasmussen, E., Rison, W., Rust, W. D., and Thomas, R. J.: The Severe Thunderstorm Electrification and Precipitation Study (STEPS), Bull. Amer. Meteor. Soc., 85, 1107–1125, 2004.

Luque, M. Y., Bürgesser, R., and Ávila, E.: Thunderstorm graupel charging in the absence of supercooled water droplets. Quarterly Journal of the Royal Meteorological Society, 142(699), 2418–2423. https://doi.org/10.1002/qj.2834, 2016.

Nuissier O., Joly, B., Ducrocq, V., Joly, A., and Arbogast, P.: A statistical downscaling to identify the large scale circulation patterns associated to heavy precipitation events over southern France. Q. J. Roy. Meteorol. Soc., 137, 1812-1827, doi:10.1002/qj.866, 2011.

MacGorman, D. R., Rust, W. D.: The Electrical Nature of Storms, Oxford University Press, New-York, 422 pp, 1998.

MacGorman, D. R., et al. (2008): TELEX: The Thunderstorm Electrification and Lightning Experiment, Bull. Am. Meteorol. Soc., 89, 997-1013, doi:10.1175/2007BAMS2352.1, 2008.

McCaul, E. W., Goodman, S. J., LaCasse, K. M., and Cecil, D. J.: Forecasting lightning threat using cloud-resolving model simulations, Weather Forecasting, 24(3), 709–729, doi:10.1175/2008WAF2222152.1, 2009.

Marshall, T. C., Rust, W. D., Winn, W. P., and Gilbert, K. E.: Electrical structure in two thunderstorm anvil clouds. J. Geophys. Res., 94(D2), 2171. doi.org/10.1029/JD094iD02p02171, 1989.

Mazur, V.: Physical processes during development of lightning flashes, C. R. Physique 3, 1393–1409, 2002.

Montanyà, J., van der Velde, O., and Williams, E. R.: The start of lightning: Evidence of bidirectional lightning initiation. Sci. Rep. 5, 15180; doi: 10.1038/srep15180, 2015.

Pinty, J.-P., Barthe, C., Defer, E., Richard, E., and Chong, M.: Explicit simulation of electrified clouds: From idealized to real case studies, Atmospheric Research, 123, 82-92, doi.org/10.1016/j.atmosres.2012.04.008, 2013.

Ribaud, J.-F., Bousquet, O., and Coquillat, S.: Relationships between total lightning activity, microphysics and kinematics during the 24 September 2012 HyMeX bow-echo system, Q. J. R. Meteorol. Soc., DOI:10.1002/qj.2756, 2016.

Saunders, C. P. R.: Charge separation mechanisms in clouds, Space Sci. Rev. 137: 335 – 353, 2008.

Scheffknecht P, Richard, E., and Lambert, D.: A highly localized high-precipitation event over Corsica. Q. J. R. Meteorol. Soc., 142, 206–221, 2016.

Stolzenburg, M., Rust, W. D., Smull, B. F., and Marshall, T. C.: Electrical structure in thunderstorms convective regions: 1. Mesoscale convective systems, J. Geophys. Res., 103, 14,059, 1998.

Stolzenburg, M., and Marshall, T. C.: Charge structure and dynamics in thunderstorms. Space Science Reviews, 137(1–4), 355–372, doi.org/10.1007/s11214-008-9338-z, 2008.

Thomas, R. J., Krehbiel, P. R., Rison, W., Harlin, J., Hamlin, T., and Campbell, N.: The LMA flash algorithm, Proceedings of the 12th International Conference on Atmospheric Electricity, 489-492, Versailles, 9-12 June, 2003.

Thomas, R.J., Krehbiel, P.R., Rison, W., Hunyady, S. J., Winn, W.P., Hamlin, T., and Harlin, J.: Accuracy of the Lightning Mapping Array, J. Geophys. Res., 109, 34 pp., D14207, doi:10.1029/2004JD004549, 2004.

Tidiga, M., Coquillat, S., Ricard, D., Defer, E., De Guibert, P., Lambert, D., Pinty, J.-P., Pont, V., and Prieur, S.: Daytime convection in Corsica in absence of synoptic forcing: fine-scale analysis of the relief and coastal breezes influence using lightning observation (SAETTA) and high-resolution numerical simulation (Meso-NH), 11th HyMeX Workshop, 29 May – 2 June, Lecce, Italie, 2018.

van der Velde, O. A., and Montanyà, J.: Asymmetries in bidirectional leader development of lightning flashes, J. Geophys. Res. Atmos., 118, 1–16, doi:10.1002/2013JD020257, 2013.